Oncogene (2004) 23, 5161–5174

www.nature.com/onc

Inhibition of *in vivo* breast cancer growth by antisense oligodeoxynucleotides to type I insulin-like growth factor receptor mRNA involves inactivation of ErbBs, PI-3K/Akt and p42/p44 MAPK signaling pathways but not modulation of progesterone receptor activity

Mariana Salatino[1], Roxana Schillaci[1], Cecilia J Proietti[1], Romina Carnevale[1], Isabel Frahm[2], Alfredo A Molinolo[1], Adolfo Iribarren[3], Eduardo H Charreau[1] and Patricia V Elizalde*[,1]

[1]*Laboratory of Molecular Mechanisms of Carcinogenesis, Instituto de Biología y Medicina Experimental (IBYME), CONICET, Obligado 2490, Buenos Aires 1428, Argentina;* [2]*Servicio de Patología, Sanatorio Mater Dei, Buenos Aires, Argentina;* [3]*Instituto de Investigaciones en Ingeniería Genética y Biología Molecular (INGEBI), Argentina*

The present study addresses the effect of targeting type I insulin-like growth factor receptor (IGF-IR) with antisense strategies in *in vivo* growth of breast cancer cells. Our research was carried out on C4HD tumors from an experimental model of hormonal carcinogenesis in which the synthetic progestin medroxyprogesterone acetate (MPA) induced mammary adenocarcinomas in Balb/c mice. We employed two different experimental strategies. With the first one we demonstrated that direct intratumor injection of phosphorothioate antisense oligodeoxynucleotides (AS[S]ODNs) to IGF-IR mRNA resulted in a significant inhibition of C4HD tumor growth. In the second experimental strategy, we assessed the effect of intravenous (i.v.) injection of AS [S]ODN on C4HD tumor growth. This systemic treatment also resulted in significant reduction in tumor growth. The antitumor effect of IGF-IR AS[S]ODNs in both experimental protocols was due to a specific antisense mechanism, since growth inhibition was dose-dependent and no abrogation of tumor proliferation was observed in mice treated with phosphorothioate sense ODNs (S[S]ODNs). In addition, IGF-IR expression was inhibited in tumors from mice receiving AS[S]ODNs, as compared to tumors from control groups. We then investigated signal transduction pathways modulated *in vivo* by AS[S]ODNs treatment. Tumors from AS[S]ODN-treated mice of both intratumoral and intravenous protocols showed a significant decrease in the degree of insulin receptor substrate-1 (IRS-1) tyrosine phosphorylation. Activation of two of the main IGF-IR signaling pathways, phosphatidylinositol 3-kinase (PI-3K)/Akt and p42/p44 mitogen-activated protein kinases (MAPK) was abolished in tumors growing in AS[S]ODN-treated animals. Moreover, ErbB-2 tyrosine phosphorylation was blocked by *in vivo* administration of AS[S]ODNs. On the other hand, we found no regulation of either progesterone receptor expression or activity by *in vivo* AS[S]ODNs administration. Our results for the first time demonstrated that breast cancer growth can be inhibited by direct *in vivo* administration of IGF-IR AS[S]ODNs.

Oncogene (2004) **23,** 5161–5174. doi:10.1038/sj.onc.1207659
Published online 3 May 2004

Keywords: breast cancer; IGF-IR; antisense strategies

Introduction

Type I insulin-like growth factor receptor (IGF-IR) plays a pivotal role in the regulation of cell growth in different ways. It is not only mitogenic for several cell types but also plays a crucial role in the establishment and maintenance of the transformed phenotype, protects cells from a variety of apoptotic signals and finally also induces differentiation of certain cell types (for review see Werner and Le Roith, 2000). Evidence of a crucial role of IGF-IR in malignant transformation was first provided by the findings of Sell *et al.* (1994), showing that mouse embryo cells with a targeted disruption of IGF-IR (R-cells) cannot be transformed by SV40T antigen and/or activated Ha-ras oncogene (Sell *et al.*, 1994) both of which easily transform embryo cells obtained from wild-type littermates. This finding has since then been confirmed with several viral and cellular oncogenes that also fail to transform R-cells (reviewed in Baserga, 1999).

A growing body of evidence indicates that IGF-IR plays a key role in breast cancer development and that it is involved in a complex cross-talk with steroid hormones that regulates breast tumor growth (reviewed in Surmacz *et al.*, 1998). High levels of IGF-IR expression have been found in breast tumors and breast cancer cell lines (reviewed in Surmacz *et al.*, 1998). However, accumulating evidence supports the hypothesis that an obligatory requirement to establish and maintain the transformed phenotype is the presence of

*Correspondence: PV Elizalde;
E-mail: elizalde@dna.uba.ar
Received 17 November 2003; revised 13 February 2004; accepted 13 February 2004; published online 3 May 2004

physiological levels of IGF-IR instead of overexpression of this receptor (reviewed in Yu and Rohan, 2000).

We have already demonstrated that IGF-IR plays a key role in the proliferation of C4HD tumors from an experimental model of hormonal carcinogenesis in which the synthetic progestin medroxyprogesterone acetate (MPA) induced mammary adenocarcinomas in female Balb/c mice. As we have previously described in detail (Elizalde *et al*., 1998; Balana *et al*., 1999, 2001), C4HD tumors are of ductal origin, require MPA administration to proliferate both *in vivo* and in *in vitro,* and express high levels of estrogen (ER) and progesterone receptors (PR) (Elizalde *et al*., 1998; Balana *et al*., 1999, 2001). C4HD tumors also express IGF-IR and synthesize IGF-I (Elizalde *et al*., 1998). In previous works, we found that blockage of IGF-IR expression by using antisense oligodeoxynucleotides (ASODNs) to IGF-IR mRNA, inhibited MPA-stimulated growth of primary cultures of epithelial cells from C4HD tumor (Elizalde *et al*., 1998), indicating that a functional autocrine loop involving IGF-I and IGF-IR participates in MPA-induced proliferation of C4HD cells. On the other hand, our studies of the expression and function of type I receptor tyrosine kinases (RTKs: EGF-R/ErbB-1, ErbB-2, ErbB-3 and ErbB-4), and their ligand, heregulin (HRG), revealed the existence of bi-directional cross-talks between progestins and HRG/Erbs signaling pathways that control C4HD cell growth (Balana *et al*., 1999, 2001). Finally, we found interaction between IGF-IR and HRG/ErbBs signaling, evidenced first by the fact that HRG induced a potent proliferative response in C4HD cells, which was completely abolished by the blockage of IGF-IR expression using ASODNs (Balana *et al*., 1999); second, by the presence of a hierarchical interaction between IGF-IR and ErbB-2, by which IGF-IR directs ErbB-2 phosphorylation (Balana *et al*., 2001). As a whole, our findings consistently identify IGF-IR as playing a key role in C4HD cell proliferation driven by three different but related pathways, that is, by the PR, by HRG/ErbBs and lastly by its own IGF-I/IGF-IR autocrine loop.

In the present study, we have assessed the effect of targeting IGF-IR with antisense strategies in *in vivo* growth of C4HD tumors. Our findings for the first time demonstrated that either direct intratumor injection or systemic administration of phosphorothioate antisense ODNs (AS[S]ODNs) to IGF-IR mRNA resulted in a significant growth inhibition of C4HD tumors. In addition, we dissected a network of interactions among IGF-IR, type I RTKs, and PR signaling pathways that were differentially affected by blockage of IGF-IR function.

Results

Effects of IGF-IR AS[S]ODNs on C4HD cell in vitro *proliferation*

The aim of the present study was to explore the effect of the abolishment of IGF-IR expression, by using ASODNs, in *in vivo* growth of C4HD tumors. To overcome the rapid degradation of the phosphodiester ODNs by nucleases, we used phosphorothioate ODNs ([S]ODNs) in the experiments carried out *in vivo*. Here, we first compared the ability of the AS[S]ODNs to IGF-IR to inhibit *in vitro* proliferation of C4HD cells with the effect of their unmodified counterparts, the phosphodiester ASODNs, which we had already used in our previous studies (Elizalde *et al*., 1998; Balana *et al*., 1999, 2001). As shown in Figure 1a, phosphorothioate AS[S]ODNs are able to exert a dose-dependent inhibition of MPA-induced C4HD cell growth, comparable to the one exerted by the phosphodiester ASODNs. Sense [S]ODNs had no effect on proliferation at any of the tested doses. The effect of IGF-IR AS[S]ODNs on protein expression was assessed by immunoblotting

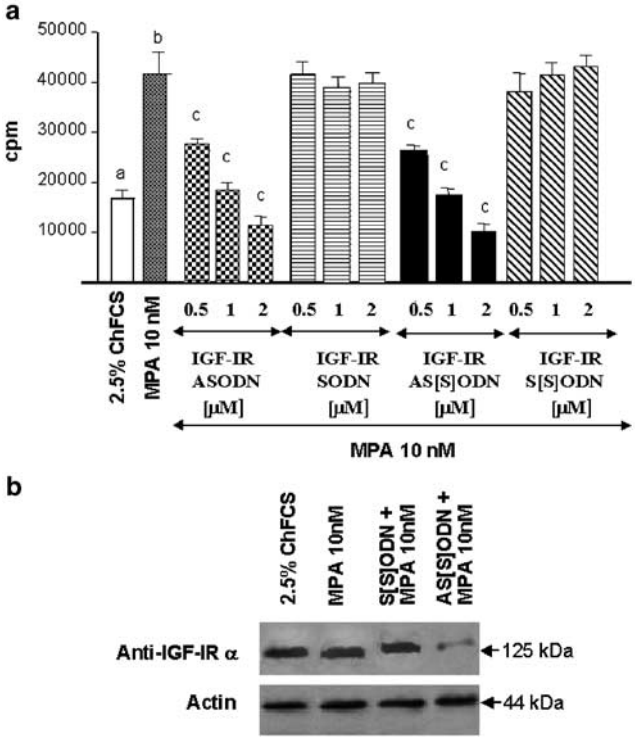

Figure 1 Inhibition of MPA-induced *in vitro* proliferation of C4HD cells by AS[S]ODNs to IGF-IR mRNA. (**a**) Primary cultures of C4HD cells were incubated for 48 h in medium with 2.5% ChFCS supplemented with MPA 10 nM, MPA + phosphophosphodiester ASODNS or SODNs, and MPA + phosphorothioosphorothioate AS[S]ODNs or S[S]ODNs to IGF-IR mRNA. Incorporation of (^{3}H)-thymidine was used as a measure of DNA synthesis. Data are presented as mean ± s.d. b vs a, and c vs b: $P<0.001$. The experiment shown is representative of a total of four. (**b**) Effect of AS[S]ODNs on IGF-IR protein synthesis. A total of 100 μg protein from C4HD cell lysates was electrophoresed and immunoblotted with an IGF-IR α chain antibody. Densitometric analysis of IGF-IR band, expressed as a percentage of the control value (i.e. C4HD cells growing in MPA10 nM) is 37% for cells treated with 2 μM AS[S]ODNs. No significant differences were found in densitometric values of IGF-IR band between control cells and cells treated with 2 μM S[S]ODNs. Western blot using an antiactin antibody was carried out using identical protein lysates as control for the specificity of the IGF-IR AS[S]ODNs. This is a representative experiment of a total of four in which s.e. was within 10%

C4HD cell lysates (Figure 1b). Densitometric evaluation demonstrated that IGF-IR levels were reduced by 60–70% after 2 μM AS[S]ODN treatment, while S[S]ODNs did not reduce IGF-IR levels (Figure 1b), confirming the specificity of the IGF-IR AS[S]ODNs. As we have previously reported using ligand-binding assays (Elizalde *et al*., 1998), MPA treatment did not regulate IGF-IR protein levels, since comparable levels of IGF-IR expression were found in C4HD cells growing in 2.5% ChFCS or treated with MPA (Figure 1b, first and second lanes).

In vivo *effects of IGF-IR AS[S]ODNs treatment on C4HD tumor growth*

All *in vivo* experimental protocols were performed in animals treated subcutaneously (s.c.) with 40 mg MPA depot in the opposite flank to tumor inoculum. To test the therapeutic effect of IGF-IR AS[S]ODNs, we first proceeded through direct intratumoral injection of [S]ODNs. MPA-treated mice were inoculated s.c. with a fragment of C4HD tumor. [S]ODN treatment started when tumors reached a mean volume of 15 mm^3. Mice were injected directly into the tumor with 100 μg/day/mouse IGF-IR AS[S]ODNs or S[S]ODNs for 14 days. As a further control, another group was injected with 100 μl PBS. Tumor width and length were measured daily, in order to calculate volume. As shown in Figure 2, AS[S]ODN treatment resulted in a significant inhibition of mean tumor volume as compared to S[S]ODN- or PBS-treated mice. Tumor growth rates, determined as the slopes of growth curves obtained during the first 15 days of this protocol, were significantly lower in AS[S]ODN-treated mice as compared to S[S]ODN-treated or PBS-treated animals (Table 1). At day 15, half the mice in each group were killed and tumors were excised. As shown in Table 1, intratumor injection of

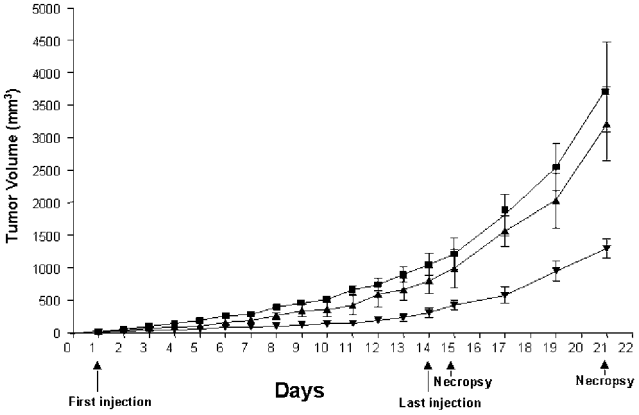

Figure 2 Effect of intratumoral injection of AS[S]ODNs to IGF-IR on C4HD mammary adenocarcinomas growth. C4HD tumors were implanted s.c. in Balb/c mice treated with 40 mg MPA depot. Treatment started when tumors reached a mean volume of 15 mm^3. Mice were injected directly into the tumor with 100 μg/day/mice AS[S]ODN (▼) ($n=10$), S[S]ODN (▲) ($n=10$), or 100 μl of PBS (■) ($n=10$) for a total of 14 days. Tumor length and width were measured daily and tumor volume was calculated as described in Material and methods. At day 15 half the animals in each group were killed and tumors were excised. Each point represents the mean volume ± s.e. of 10 independent tumors during the first 15 days and of five tumors during days 16–21

Table 1 Effect of intratumor and systemic administration of AS[S]ODNs on C4HD tumor growth

	Day 15			*Day 21*		
Treatment	*Tumor volume (mm^3) (mean ± s.e.)*	*Growth rate (mm^3/day)*	*AS[S]ODN growth inhibition (%)*	*Tumor volume (mm^3) (mean ± s.e.)*	*Growth rate (mm^3/day)*	*AS[S]ODN growth inhibition (%)*
Intratumor						
100 μg/day/mouse	AS: 409.0 ± 3.5[a]	AS: 22.4 ± 2.6[a]	*Respect to:*	AS: 1255.0 ± 44.6[a]	AS: 153.8 ± 16.7[a]	*Respect to:*
	S: 1104.0 ± 128.1[b]	S: 70.0 ± 6.2[c]	S: 62.3	S: 3524.0 ± 342.0[c]	S: 357.4 ± 99.4[c]	S: 64.4
	PBS: 1213.0 ± 160.2[c]	PBS: 81.4 ± 5.4[c]	PBS: 66.3	PBS: 3771.0 ± 447.4[c]	PBS: 288.4 ± 95.8[c]	PBS: 66.7
Intravenous low dose						
0.25 mg/day/mouse (1–7)	AS: 670.7 ± 20.3[a]	AS: 50.5 ± 2.0[a]	*Respect to:*	AS: 1067.0 ± 55.8[a]	AS: 61.8 ± 7.3[a]	*Respect to:*
0.5 mg/day/mouse (9–11–13)	S: 1433.0 ± 178.3[c]	S: 106.0 ± 5.2[c]	S: 53.2	S: 2255.0 ± 181.5[c]	S: 146.5 ± 29.1[c]	S: 52.7
1 mg/day/mouse (8–10–12–14)	PBS: 1504.0 ± 57.5[c]	PBS: 115.3 ± 6.0[c]	PBS: 55.4	PBS: 2554.0 ± 19.0[c]	PBS: 177.9 ± 9.4[c]	PBS: 58.2
Intravenous high dose						
1 mg/day/mouse	AS: 444.0 ± 58.9[a,†]	AS: 20.2 ± 1.4[a,*]	*Respect to:*	AS: 775.0 ± 100.0[a]	AS: 52.6 ± 5.8[a]	*Respect to:*
	S: 1165.0 ± 92.6[c]	S: 61.6 ± 3.3[c]	S: 62.0	S: 2167.0 ± 138.2[c]	S: 167.4 ± 40.9[c]	S: 64.2
	PBS: 1304.0 ± 57.1[c]	PBS: 64.3 ± 4.6[c]	PBS: 66.0	PBS: 2230.0 ± 134.0[c]	PBS: 166.0 ± 19.2[c]	PBS: 65.2

All experimental protocols were performed in mice treated with 40 mg s.c. MPA depot in the opposite flank to tumor inoculum. Mice were treated when tumors reached 15 mm^3. Each group contained 10 mice. Growth rate between day 1 and 15 was calculated as the slopes of growth curves. At day 15, one day after last injection in all three protocols, tumor volume and percentage of growth inhibition in tumors from AS[S]ODNs-treated mice (AS) with respect to either S[S]ODNs (S) or PBS treated animals was calculated as described in Materials and methods. At this point, half the mice in each group were killed and tumors were excised. The other half of mice in each experimental group were kept alive for one more week after the end of the treatment. Growth rates were calculated as the slope of growth curves from days 15 to 21. Tumor volume and percentage of growth inhibition in tumors from AS[S]ODNs-treated mice (AS) with respect to either S[S]ODNs (S)- or PBS-treated animals at day 21 are shown. a vs b $P<0.01$; a vs c $P<0.001$; $^{\dagger}P<0.001$ in comparison with tumor volume in AS-treated animals from the intravenous low-dose treatment; $^{*}P<0.001$ in comparison with growth rate of AS-treated tumors from the low-dose treatment

AS[S]ODNs significantly inhibited C4HD tumor growth, determined by comparing mean tumor volume of AS[S]ODN-treated mice with tumor volume of either S[S]ODN- or PBS-treated mice. Tumor growth delay at day 15 was of 5 days with respect to S[S]ODN-treated mice and of 7 days with respect to PBS-treated animals. The other half of mice in each experimental group was kept alive for one more week after the end of the treatment. Differences in tumor growth and growth rates between AS[S]ODN-treated mice and S[S]ODN- or PBS-treated control groups were still significant at day 21 (Table 1).

Systemic treatment of solid tumors with antisense oligonucleotides is currently under investigation in several trials (Tamm *et al*., 2001). Therefore, positive results obtained in the intratumoral protocol encouraged us to assess the effect of intravenous (i.v.) injection of AS[S]ODNs on C4HD tumor growth. In the first series of experiments, mice were injected i.v. via the retroorbital venous sinus, with 0.25 mg/day/mouse AS[S]ODNs or S[S]ODNs for 7 days. A third group was inoculated with the vehicle (100 μl PBS). From now on, we will be referring to this experimental approach as low-dose protocol. As shown in Figure 3a (inset), AS[S]ODN treatment for 7 days induced a detectable but not significant decrease in tumor growth. Therefore, we decided to raise the dose to 1 mg/day/mouse of AS[S]ODNs or S[S]ODNs on days 8, 10, 12 and 14 and to 0.5 mg/day/mouse of oligonucleotides on days 9, 11 and 13. This treatment modification resulted in a marked reduction in tumor volume in AS[S]ODN-treated mice, as compared with either S[S]ODN or PBS control groups (Figure 3a). At day 15, half the animals in each group were killed and tumors were excised. Results are summarized in Table 1. AS[S]ODN treatment induced significant decrease both in tumor growth and in growth rates. At day 15, a delay of 6 days in tumor growth was observed in mice treated with AS[S]ODNs with respect to tumors growing in either S[S]ODN- or PBS-treated animals. In an effort to improve treatment with systemic AS[S]ODNs in the last experimental design, which we will be referring to as high-dose protocol, we rose [S]ODNs dose to 1 mg/day/mouse from day 1 to day 14 of treatment. As seen in Figure 3b, the inhibitory effect of AS[S]ODNs was evident from the beginning of the treatment. This systemic treatment proved to be highly effective to inhibit tumor growth (Table 1). A delay of 6 days in tumor growth with respect to S[S]ODN and PBS administration was observed at day 15 when, as described for the other two therapeutic schedules, tumors were excised from half the mice in each group. As already seen in the intratumoral protocol, in both intravenous protocols, differences observed in tumor growth and in growth rates were evident and significant 1 week after the end of the treatment on day 21 (Table 1). No statistically significant differences either in tumor growth, in growth rates or in growth delay between S[S]ODN and PBS control groups were observed in any of the experimental schedules (Table 1).

There were no signs of overt toxicity in mice treated with AS[S]ODNs either in intratumoral or in intravenous experiments and no significant changes in serum levels of aspartate aminotransferase (AST), alanine aminotransferase (ALT), glucose and creatinin were found between AS[S]ODN-treated and control groups (data not shown). In addition, we did not observe weight loss in mice receiving AS[S]ODNs in any of the three experimental protocols which evidences good tolerance by animals of the three experimental regimens.

Histhopathogical analysis

Morphology of tumors from AS[S]ODN-, S[S]ODN- or PBS-treated mice was evaluated by haematoxylin–eosin (H&E) staining of histological sections. Tumors were excised at day 15 of each protocol. Figure 4 shows representative sections of tumors from AS[S]ODNs, S[S]ODNs and PBS-treated mice in the high-dose intravenous experimental protocol. A large percentage, about 70–90%, of tumor mass from AS[S]ODN-treated mice was necrotic as compared to S[S]ODN- or PBS-treated mice, in which only 10–20% necrosis was observed. Tumors from mice receiving AS[S]ODNs showed a significantly lower number of mitosis (0–5 mitosis per 10 HPF) as compared to S[S]ODN- or PBS-treated animals, both of which showed over 10 mitoses per 10 HPF. Histopathological images of tumors from the intratumoral or low-dose intravenous protocols were similar to those observed in the high-dose treatment group (data not shown). In addition, histological examination of liver, lung, heart and pancreas did not reveal any pathological changes (data not shown).

Molecular mechanisms involved in the antitumoral effect of IGF-IR AS[S]ODNs

Since we achieved a significant though incomplete inhibition of C4HD tumor growth by IGF-IR AS[S]ODN administration, we had tumor samples available to explore signaling pathways disrupted *in vivo* by targeting IGF-IR.

To establish first whether the antitumor effect *in vivo* was due to a specific antisense effect, IGF-IR expression in tumors from AS[S]ODN-, S[S]ODN- and PBS-treated mice was evaluated in protein extracts from tumors excised at day 15. As control, we included C4HD tumors growing in MPA-untreated animals (Figure 5a, MPA-U). As shown in Figure 5a, Western blot analysis showed a marked inhibition of IGF-IRα chain expressions in tumors from mice receiving AS[S]ODNs, as compared with tumors from S[S]ODN- or PBS-treated animals, in the intratumor and in both low-dose and high-dose i.v. therapeutic schedules. Densitometric analysis of IGF-IR α chain band in tumor samples from PBS-, S[S]ODN- and AS[S]ODN-treated mice showed that AS[S]ODN treatment resulted in 65–90% inhibition of IGF-IR α chain expression with respect to tumors growing in control groups in all three therapeutic protocols. Similar results on AS[S]ODN treatment inhibition of IGF-IRβ chain expression were found

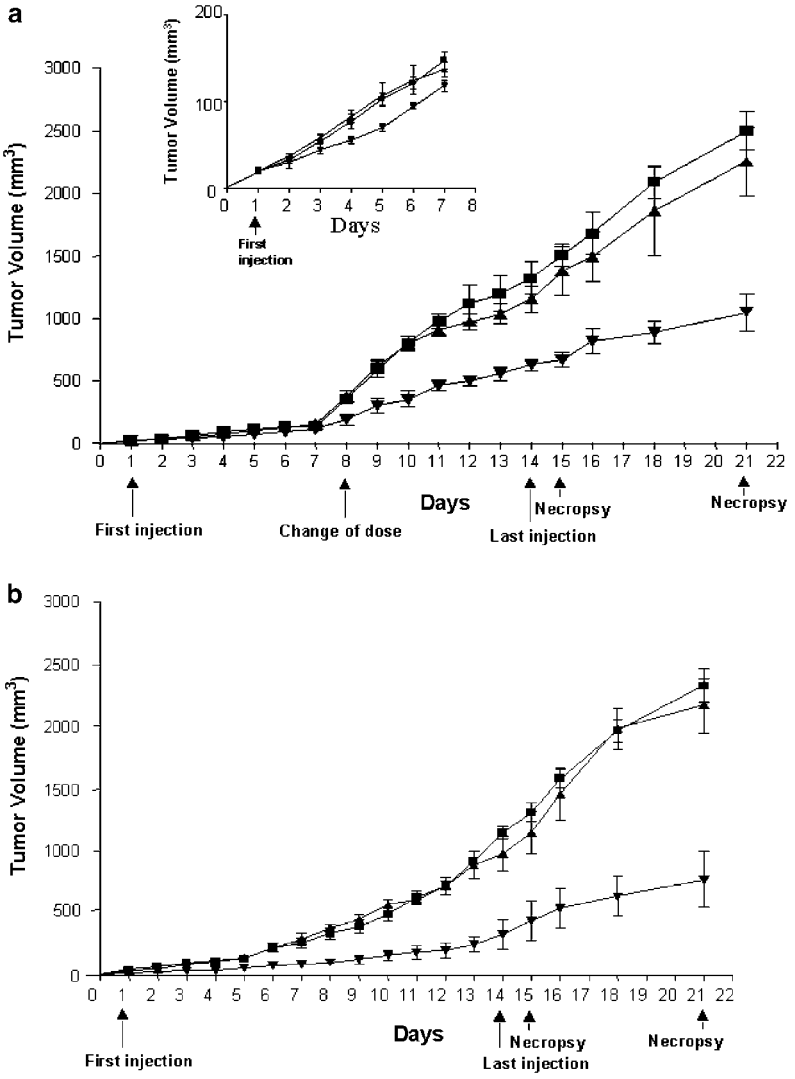

Figure 3 Effect of intravenous (i.v.) injection of AS[S]ODNs to IGF-IR on C4HD tumor growth. (**a**) Low-dose protocol. MPA-treated mice bearing C4HD tumors of 15 mm^3 were injected i.v. with 0.25 mg/day/mouse AS[S]ODN (▼) ($n=10$), 0.25 mg/day/mouse of S[S]ODN ($n=10$) (▲) or PBS ($n=10$) (■) for the fist 7 days, and then dose was raised to 1 mg/day/mouse AS[S]ODN (▼) or S[S]ODN (▲) on days 8, 10, 12 and 14, and to 0.5 mg/day/mouse of either AS[S]ODN (▼) or S[S]ODN (▲) on days 9, 11 and 13. Inset shows the first 7 days of treatment. Mean tumor volumes were calculated daily as described in Materials and methods. At day 15 half the animals in each group were killed and tumors were excised. Each point represents the mean volume ±s.e. of 10 independent tumors during the first 15 days and of five tumors during days 16–21. (**b**) High-dose protocol. MPA-treated mice bearing C4HD tumors of 15 mm^3 were injected i.v. with 1 mg/day/mouse AS[S]ODN (▼) ($n=10$), 1 mg/day/mouse S[S]ODN ($n=10$) (▲) or PBS ($n=10$) (■) during 14 days. Mean tumor volumes were calculated daily. At day 15 half the animals in each group were killed and tumors were excised. Each point represents the mean volume ±s.e. of 10 independent tumors during the first 15 days and of five tumors during days 16–21

(data not shown). IGF-IR β chain tyrosine phosphorylation was readily detectable in tumors growing in PBS-, and S[S]ODN-treated mice from the intravenous high-dose protocol (Figure 5b). In addition, we are showing that IGF-IR β chain is tyrosine phosphorylated in C4HD tumors from MPA-untreated animals (Figure 5b, MPA-U lane). This was an expected result since both MPA-treated and -untreated tumors express same levels of IGF-IR and synthesize same amount of IGF-I (Elizalde *et al*., 1998). Therefore, this autocrine loop is responsible for the activation of IGF-IR in both MPA-treated and -untreated tumors. As shown in Figure 5b, IGF-IR β chain tyrosine phosphorylation dramatically decreased in tumors from AS[S]ODN-treated mice of the intravenous high-dose protocol (Figure 5b). Similar results were found in the intratumor and the intravenous low-dose therapeutic schedules (data not shown).

An essential step in signal transduction from IGF-IR is the phosphorylation of insulin receptor substrate-1 (IRS-1). Of the downstream signals activated by IRS-1, the best characterized is the PI-3K/Akt pathway (Backer *et al*., 1993; Scrimgeour *et al*., 1997 and references within). Here, we assessed IRS-1 phosphorylation state and PI-3K/Akt activation as a way to identify signaling pathways affected *in vivo* by the abolishment of IGF-IR

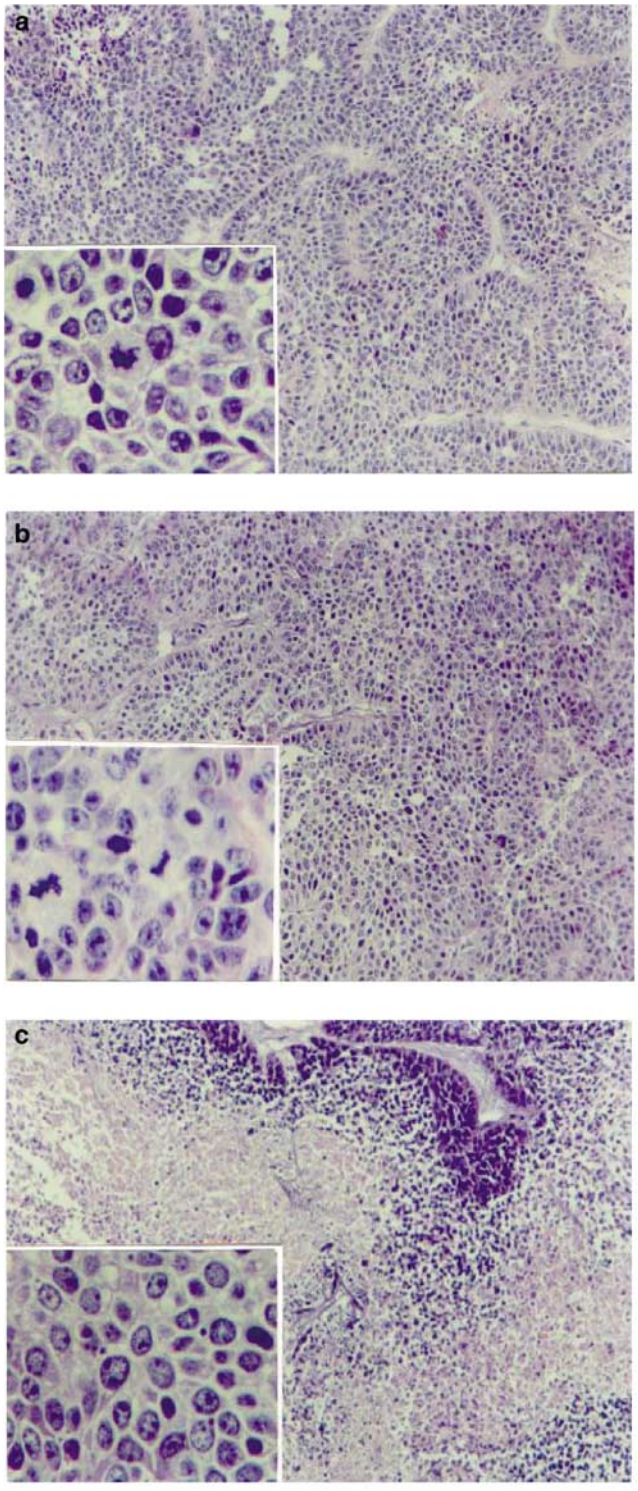

Figure 4 Histopathological analyses. (**a** and **b**) Tissue sections of tumors from PBS- and S[S]ODN-treated mice, respectively. Ductal carcinoma composed of pseudolobules of highly cohesive glandular cells, separated by scanty vascular stroma (H&E $\times 100$). Atypical features and several mitotic figures are evident at higher magnification (inset, H&E $\times 400$). (**c**) Tissue sections of tumors from AS[S]ODN-treated tumors. Highly necrotic tumor disclosing few remaining cells (H&E $\times 100$). In non-necrotic areas the tumor shows the absence of mitosis (inset, H&E $\times 400$)

expression. IRS-1 tyrosine phosphorylation was detected in both PBS and S[S]ODN control groups from all three experimental protocols (Figure 6a, upper panels in each protocol). In addition, IRS-1 tyrosine phosphorylation was found in tumors from MPA-untreated mice (Figure 6a, upper panel, MPA-U lane), in accordance with the activation of IGF-IR observed in these tumors. Significant decrease in the degree of IRS-1 tyrosine phosphorylation (Figure 6a, upper panels in each treatment) was found in tumors from AS[S]ODN-treated mice of both intratumoral and intravenous protocols, as compared to tumors growing in both control groups. To investigate the PI-3K/Akt activation status, we performed Western blots with anti-phospho-Akt threonine 308 and anti-phospho-Akt serine 473 antibodies, as markers of Akt activation. As shown in Figure 6b, a significant decrease in both Akt threonine 308 and serine 473 phosphorylation was detected in tumors from AS[S]ODN-treated mice with respect to tumors growing in PBS- or in S[S]ODN-treated animals in all experimental schedules. Figure 6b also shows that tumors growing in MPA-untreated mice (MPA-U lane) display significantly lower levels of Akt activation as compared to tumors growing in MPA-treated animals from the PBS and S[S]ODN control groups in all three protocols.

We had already shown the existence of a hierarchical interaction between IGF-IR and ErbB-2, by means of which IGF-IR directs ErbB-2 phosphorylation in breast cancer cells (Balana *et al*., 2001), and had already reported that blockage of IGF-IR with ASODNs did not affect the levels of ErbB-2 protein expression in primary cultures of C4HD cells (Balana *et al*., 1999). In our current study, we found that AS[S]ODNs did not regulate ErbB-2 content *in vivo* in any of the protocols and also found that ErbB-3 levels remained unaffected by AS[S]ODN treatment (data not shown). We then assessed ErbB-2 and ErbB-3 phosphorylation state in tumors obtained from all three experimental regimens, as a marker of their activation. As we have already found in C4HD tumors growing in MPA-treated mice (Balana *et al*., 1999, 2001), we detected a strong degree of ErbB-2 and ErbB-3 tyrosine phosphorylation in both PBS and S[S]ODN control groups (Figure 7a, upper panels in each protocol, lanes 1, 2, 4 and 5). Tumors from AS[S]ODN-treated mice of both intratumoral and intravenous protocols showed a significant decrease in the degree of both ErbB-2 and ErbB-3 tyrosine phosphorylation as compared to tumors growing in S[S]ODN- or in PBS-treated mice (Figure 7a, upper panels in each treatment, lanes 3 and 6). These findings provide the first demonstration that blockage of IGF-IR expression *in vivo* leads to inhibition of ErbB-2 and ErbB-3 tyrosine phosphorylation. The presence of heterodimers between ErbB-2 and ErbB-3 was investigated by immunoprecipitating tumor extracts with an anti-ErbB-2 antibody and by revealing Western blots with an anti-ErbB-3 antibody. Figure 7b shows that while heterodimers between ErbB-2 and ErbB-3 are readily detectable in PBS- and in S[S]ODN-treated mice (upper panels in each protocol, lanes 1 and 2), a

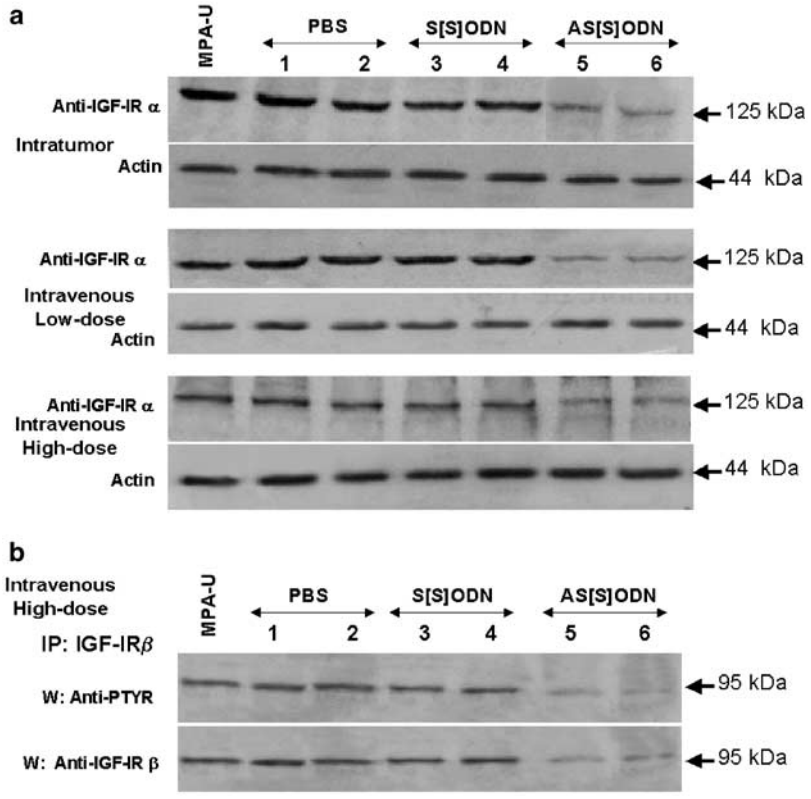

Figure 5 Effect of IGF-IR AS[S]ODNs treatment on IGF-IR expression. (**a**) A total of 100 μg protein from tumor lysates was electrophoresed and immunoblotted with an anti-IGF-IR α chain antibody. Two representative samples of mice treated with PBS (lanes 1 and 2), S[S]ODN (lanes 3 and 4) and AS[S]ODN (lanes 5 and 6) are shown. MPA-U, a representative C4HD tumor growing in MPA-untreated mouse. Western blots using an antiactin antibody were carried out using identical protein lysates as control for the specificity of the IGF-IR AS[S]ODNs (lower panels in each protocol). Densitometric analysis of IGF-IRα band from multiple AS[S]ODN-treated C4HD tumors, expressed as a percentage of the control values (i.e. C4HD tumors growing in PBS or S[S]ODN-treated mice) varied between 10 and 35% for tumors growing in AS[S]ODNs-treated animals. Inhibition of IGF-IRα expression in AS[S]ODNs-treated mice with respect to PBS or S[S]ODN-treated animals was significant ($P<0.001$). (**b**) IGF-IR β chain was immunoprecipitated from 500 μg of protein extracts and immunocomplexes were subjected to SDS–PAGE and analysed by Western blotting with an anti-P-Tyr mAb. Lower panel: Identical aliquots of each immunoprecipitate were subjected to immunoblot analysis with anti-IGF-IR β chain antibody to verify that nearly equal amount of immunoprecipitated proteins were loaded. Two representative samples of mice treated with PBS (lanes 1 and 2), S[S]ODN (lanes 3 and 4) and AS[S]ODN (lanes 5 and 6) are shown. MPA-U, a sample from C4HD tumor growing in MPA-untreated mouse. This is a representative experiment out of a total of three. Densitometric analysis of IGF-IR β chain tyrosine phosphorylation from multiple AS[S]ODN-treated C4HD tumors, and from multiple C4HD tumors growing in PBS or S[S]ODN-treated mice showed that decrease in IGF-IR β tyrosine phosphorylation in AS[S]ODNs-treated mice with respect to PBS or S[S]ODN-treated animals was significant ($P<0.001$). W: Western blot, IP: Immunoprecipitation

significant decrease in the abundance of these complexes is observed in tumors growing in AS[S]ODN-treated mice (upper panels in each treatment, lane 3). Similar results were found when tumor extracts were immunoprecipitated with an anti-ErbB-3 antibody, and Western blotting was performed with an anti-ErbB-2 antibody (data not shown).

We were then for several reasons interested in assessing the effect of IGF-IR AS[S]ODNs on mitogen-activated protein kinases (MAPK) activity. First, it is well acknowledged that IGF-IR activates the MAPK/Erk signaling pathway, mainly through Shc proteins, another IGF-IR major substrate (Scrimgeour *et al*., 1997 and references within, Sasaoka *et al*., 1994). Second, the key proliferative stimulus in our tumor model is driven by MPA acting through the PR. Multiple lines of evidence, including our own work (Labriola *et al*., 2003), suggest that MAPK-induced phosphorylation plays a role in PR function (Lange *et al*., 2000; Shen *et al*., 2001; Qiu *et al*., 2003). Finally, breast cancer often shows elevated MAPK activity that has been associated to loss of estrogen response and development of metastasis (Adeyinka *et al*., 2002). Figure 8 shows results of the intravenous high-dose protocol. All tumors expressed p42/p44 MAPK (lower panel). MAPKs activation was readily detectable in tumors from control groups by performing Western blot using an antibody specific for the dually phosphorylated, active form of this kinase (Figure 8, upper panel). Tumors from AS[S]ODN-treated mice showed a significant decrease in the degree of MAPK activation as compared to tumors growing in control groups (Figure 8, upper panel). Similar results were found in the other experimental regimens (data not shown). Figure 8 also shows that tumors growing in MPA-untreated mice (MPA-U lane) display significantly lower

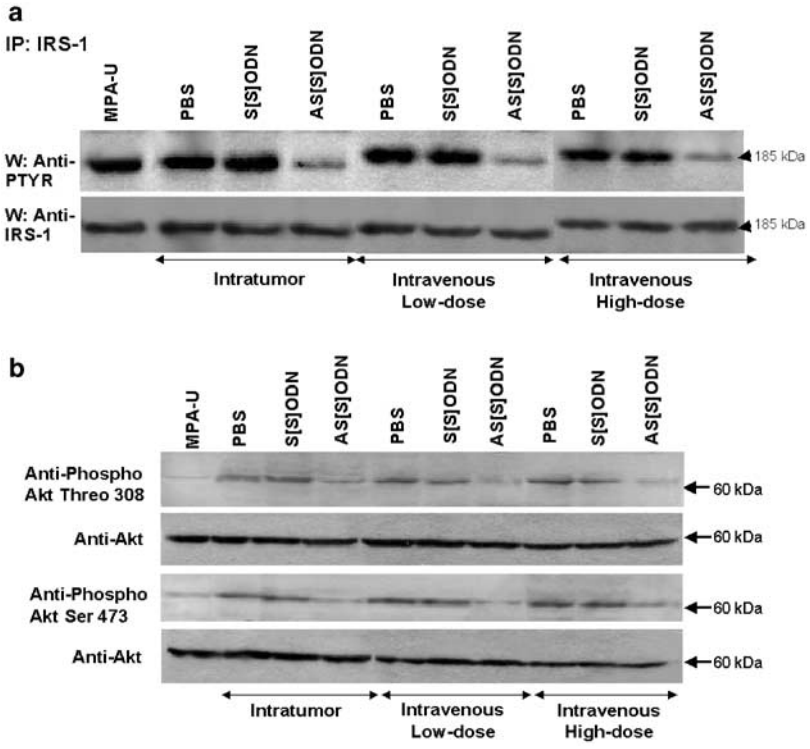

Figure 6 Effects of IGF-IR AS[S]ODNs treatment on IRS-1 and Akt phosphorylation. (**a**) Upper panel: IRS-1 was immunoprecipitated from 500 μg of protein extracts and immunocomplexes were subjected to SDS–PAGE and analysed by Western blotting with an anti-P-Tyr mAb. Lower panel: Identical aliquots of each immunoprecipitate were subjected to immunoblot analysis with anti-IRS-1 antibody to verify that nearly equal amount of immunoprecipitated proteins were loaded. A representative sample of tumors growing in mice treated with PBS, S[S]ODN and AS[S]ODN is shown. MPA-U, a sample from C4HD tumor growing in MPA-untreated mouse. This is a representative experiment out of a total of three. Densitometric analysis of IRS-1 phosphorylated bands from multiple AS[S]ODN-treated C4HD tumors, and from multiple C4HD tumors growing in PBS or S[S]ODN-treated mice showed that decrease in IRS-1 tyrosine phosphorylation in AS[S]ODNs-treated mice with respect to PBS or S[S]ODN-treated animals was significant ($P<0.001$).W: Western blot, IP: Immunoprecipitation. (**b**) A total of 100 μg protein from tumor lysates was electrophoresed and immunoblotted either with an anti-phospho-Akt threonine 308 (first panel) or with serine 473 antibody (third panel). Membranes were then stripped and hybridized with an antibody anti-total Akt (second and fourth panels). A representative sample of tumors growing in mice treated with PBS, S[S]ODN and AS[S]ODN in each protocol is shown. MPA-U, a sample from C4HD tumor growing in MPA-untreated mouse. This experiment was repeated three times with similar results. Densitometric analysis of phospho-threonine 308 or -serine 473 Akt bands from multiple AS[S]ODN-treated C4HD tumors, and from multiple C4HD tumors growing in PBS or S[S]ODN-treated mice showed that decrease in Akt tyrosine phosphorylation in AS[S]ODNs-treated mice with respect to PBS or S[S]ODN-treated animals was significant ($P<0.001$)

levels of MAPK activation as compared to tumors growing in MPA-treated animals from the PBS (lanes 1 and 2) and S[S]ODN control groups (lanes 3 and 4). This is in accordance with our previous results demonstrating that MPA induces MAPK activation *in vitro* (Labriola *et al*., 2003).

Recent evidence has clearly shown the presence of bi-directional cross-talks between steroid hormones and growth factors (GFs) signaling pathways (Ignar-Trowbridge *et al*., 1992; Pietras *et al*., 1995; Lange *et al*., 1998; Migliaccio *et al*., 1998; Balana *et al*., 1999, 2001; Boonyaratanakornkit *et al*., 2001; Shen *et al*., 2001; Labriola *et al*., 2003). Accumulating evidence has demonstrated interactions between ER and IGF-I/IGF-IR signaling pathways (Stewart *et al*., 1990; Lee *et al*., 1999; Oesterreich *et al*., 2001). However, less information is available about cross-talks between IGF-IR and PR (Katzenellenbogen and Norman, 1990; Cho *et al*., 1994; Cui *et al*., 2003). Therefore, we next investigated whether blockage of IGF-IR expression might affect PR expression and/or activity. First, we evaluated PR expression levels. The results obtained in the intravenous high-dose protocol are shown in Figure 9. Similar PR protein levels were detected in tumors from mice treated with AS[S]ODNs (lower panel, lanes 5 and 6) as compared to those found in tumors from control groups (lower panel, lanes 1–4). Same results were found in the other therapeutic schedules (data not shown). Recent findings by Lange and co-workers (Lange *et al*., 2000; Shen *et al*., 2001) demonstrated that phosphorylation of PR on Ser294 directly correlates with PR transcriptional activity. Therefore, we herein assessed the state of PR Ser294 phosphorylation in an attempt to evaluate whether abrogation of IGF-I/IGF-IR signaling could interfere with the activation of PR. As shown in Figure 9, PR phosphorylation on Ser294 was detected in PBS and S[S]ODN control groups (upper panel, lanes 1–4), in accordance with our previous *in vitro* findings, demonstrating that MPA was able to induce PR Ser294

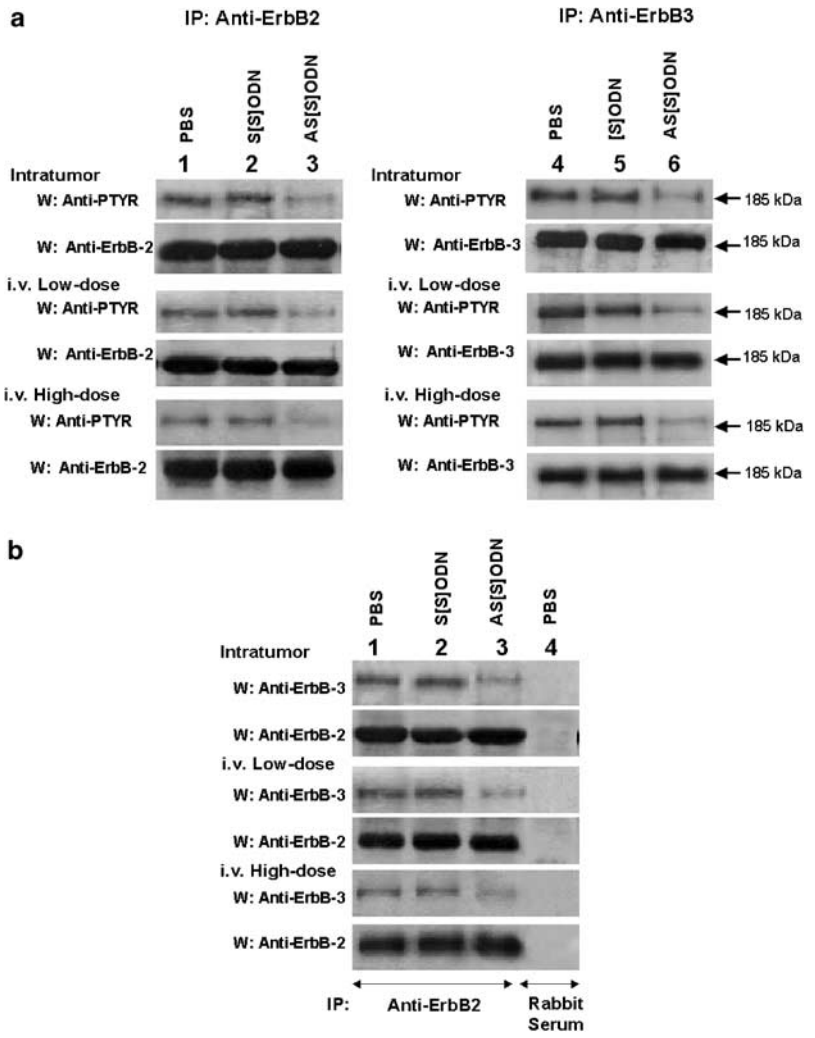

Figure 7 Effects of IGF-IR AS[S]ODNs treatment on ErbB-2 and ErbB-3 activation and heterodimerization. (**a**) ErbB-2 (right panels) and ErbB-3 (left panels) were immunoprecipitated from 500 μg of protein extracts, and immunocomplexes were subjected to SDS–PAGE and analysed by Western blotting with an anti-P-Tyr mAb. Membranes were then stripped and and hybridized with anti-ErbB-2 or ErbB-3 antibodies (lower panels in each protocol). A representative sample of mice treated with PBS (lanes 1 and 4), S[S]ODN (lanes 2 and 5) and AS[S]ODN (lanes 3 and 6) is shown. This is a representative experiment out of a total of three performed for either ErbB-2 or ErbB-3. Densitometric analysis of ErbB-2 or ErbB-3 phosphorylated bands from multiple AS[S]ODN-treated C4HD tumors, and multiple C4HD tumors growing in PBS or S[S]ODN-treated mice showed that decrease in ErbB-2 and ErbB-3 tyrosine phosphorylation in AS[S]ODNs-treated mice with respect to PBS or S[S]ODN-treated animals was significant ($P<0.001$). (**b**) Tumor extracts (500 μg) were immunoprecipitated with an ErbB-2 antibody, and immunocomplexes were subjected to electrophoresis and analysed by Western blotting with an ErbB-3 antibody. Membranes shown in upper panels of each protocol were stripped and hybridized with an anti-ErbB-2 antibody (lower panels). In lane 4, as control, 500 μg of protein extracts from tumors growing in PBS-treated mice were incubated with preimmune rabbit serum, and then Western blot was performed with anti-ErbB-2 and ErbB-3 antibodies. W: Western blot, IP: Immunoprecipitation

phosphorylation (Labriola *et al*., 2003). Tumors from AS[S]ODN-treated mice (upper panel, lanes 5 and 6), showed levels of Ser294 phosphorylation comparable to those found in control groups. We could not detect Ser294 phosphorylation of the PRA isoform in these *in vivo* tumor samples. This might be explained by the fact that, as previously reported (Clemm *et al*., 2000), anti-Ser294 antibody exhibited strong preferential reactivity for PRB. Same results were found in the other experimental protocols (data not shown). We found our result with PR particularly remarkable for it indicates that C4HD tumor cells display high levels of PR Ser294 phosphorylation in spite of IGF-IR expression blockage, which leads to a significant decrease of MAPK activity (Figure 8). Since a key feature of our model system is that blockage of IGF-IR expression proceeds in the continuos presence of MPA, this finding suggests that ligand-induced PR Ser294 phosphorylation occurs via MAPK-independent pathways.

Discussion

In the present study we have demonstrated that either intratumor or systemic administration of phosphorothioate antisense ODNs to IGF-IR mRNA resulted in

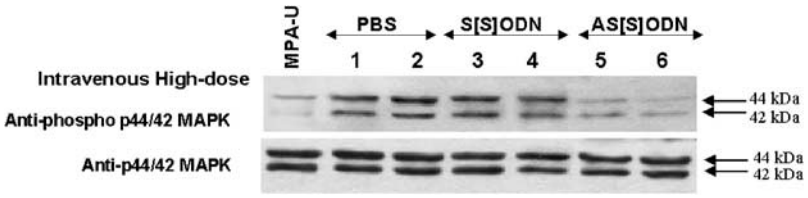

Figure 8 Effects of IGF-IR AS[S]ODNs treatment on MAPK activation. In total, 100 μg protein from tumor lysates was electrophoresed on 12% SDS gels and immunoblotted with an antiphospho p42/p44 MAPK antibody. The membrane was then stripped and hybridized with an anti-total p42/p44 MAPK antibody (lower panel). Two representative samples from mice treated with PBS (lanes 1 and 2), S[S]ODN (lanes 3 and 4) and AS[S]ODN (lanes 5 and 6) are shown. MPA-U, a sample from C4HD tumor growing in MPA-untreated mouse. This is a representative experiment out of a total of three. Densitometric analysis of phospho-MAPK showed that decrease in MAPK tyrosine phosphorylation in AS[S]ODNs-treated mice with respect to PBS or S[S]ODN-treated animals was significant ($P<0.001$)

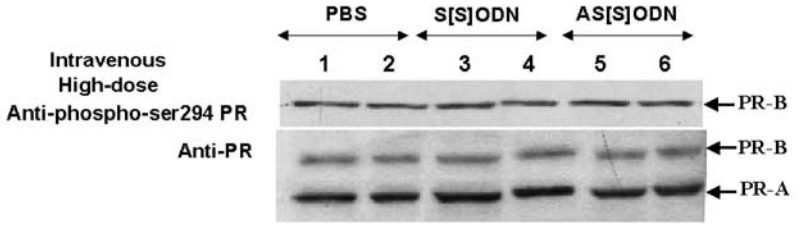

Figure 9 Effects of IGF-IR AS[S]ODNs treatment on PR expression and PR Ser294 phosphorylation. A total of 100 μg protein from tumor lysates was immunoblotted with an anti-phospho Ser 294hPR antibody (upper panel). The membrane was stripped and hybridized with an anti-hPR antibody (lower panel). Two representative samples of mice treated with PBS (lanes 1 and 2), S[S]ODN (lanes 3 and 4) and AS[S]ODN (lanes 5 and 6) are shown. This is a representative experiment out of a total of three

a significant growth inhibition of the C4HD mouse mammary tumor line, our experimental model of mammary carcinogenesis in which progestins are the major proliferative stimulus. We had previously found that progestins-induced proliferation of C4HD tumors is driven by a complex bi-directional interaction among activated PR and type I and II RTKs (Balana *et al*., 1999, 2001; Labriola *et al*., 2003). Here, we dissected a network of interactions among IGF-IR, type I RTKs and PR signaling pathways that were differentially affected by blockage of IGF-IR function Therefore, our model system has provided a unique tool to explore the molecular bases of IGF-IR contribution to breast cancer growth.

A series of experimental strategies have been employed to block either IGF-IR function or expression, both *in vitro* and *in vivo*, in several tumor cell lines derived from a number of species. These included the use of neutralizing antibodies (Rohlik *et al*., 1987; Arteaga and Osborne, 1989), dominant-negative receptors (Prager *et al*., 1994; Dunn *et al*., 1998; Li *et al*., 2000; Lee *et al*., 2003), antisense and triple-helix-forming oligonucleotides (Resnicoff *et al*., 1994a, b) and antisense expression vectors delivered by transfection or adenovirus (Resnicoff *et al*., 1994a, b; Burfeind *et al*., 1996; Lee *et al*., 1996; Nakamura *et al*., 2000). Startling reports from Baserga and co-workers (Resnicoff *et al*., 1994a, b) demonstrated that either transfection of cells with plasmids that express antisense RNA to IGF-IR or addition of ASODNs to IGF-IR mRNA were efficient at inhibiting *in vitro* growth of rat glioblastoma C6 cells. In addition, C6 cells stably transfected with a plasmid expressing antisense IGF-IR RNA were nontumorigenic when injected s.c. into syngeneic immunocompetent rats (Resnicoff *et al*., 1994a, b). Similarly, growth of human melanoma FO-1 cells in nude mice was strongly inhibited when cells stably expressed antisense IGF-IR RNA (Resnicoff *et al*., 1994a). Inhibition of tumorigenesis was also found when FO-1 cells were treated with ASODNs to IGF-IR mRNA prior to injection into nude mice (Resnicoff *et al*., 1994a).

The effect of blockage of IGF-IR function by antisense techniques in breast cancer cell has been assessed in several reports. Thus, stable expression of type I IGF-IR antisense RNA by using a plasmid vector resulted in a significant decrease in IGF-I and serum-stimulated growth in MCF-7 human breast cancer cells (Neuenschwander *et al*., 1995). In addition, recent findings demonstrated that transfection of the highly metastatic, ER negative, MDA-MB-435s breast cancer cell line with a construct carrying antisense IGF-IR RNA resulted in a significant reduction of cell proliferation and loss of soft agar growth (Chernicky *et al*., 2000). Moreover, there was suppression of tumorigenesis, reduction in the metastatic potential and prolonged survival after injection of MDA-MB-435 s cells expressing antisense IGF-IR into the mammary fat pads of immune compromised mice (Chernicky *et al*., 2000). Recently, it was found that the murine mammary carcinoma cell line EMT6 transfected with an antisense IGF-IR plasmid, displayed a significant decrease in proliferation (Chernicky *et al*., 2002). Tumor size decreased when cells carrying the antisense IGF-IR were injected into syngeneic mice (Chernicky *et al*., 2002).

It is worth pointing out that in the aforementioned studies, antisense RNA was produced intracellularly by an expression vector, in contrast to our present study in which we either injected ASODNs directly into tumors growing in mice or delivered the oligodeoxynucleotides by systemic administration through the retroorbital venous plexus. Another important difference between these studies and our present work is that most previous reports have relied on modification of cells *ex vivo* before inoculation to mice. Direct transmission of DNA into established tumors has proved to be feasible and safe at reducing tumor growth in experimental procedures in mice (Plautz *et al*., 1993) and in human clinical studies (Nabel *et al*., 1993). Though to our knowledge direct injection of ASODNs to IGF-IR in mouse mammary tumors has not been previously performed, direct injection of antisense IGF-IR plasmids into established N2A tumors growing in syngeneic A/J mice resulted in marked inhibition of tumor growth (Liu *et al*., 1998). As we have reported here, this effect persisted after the period of active DNA administration.

We have herein demonstrated that the antitumor effect of IGF-IR AS[S]ODNs was due to a specific antisense effect. First, inhibition of tumor growth by AS[S]ODNs was dose-dependent, and no abrogation of tumor proliferation was observed in any of the control groups. Thus, we found a significantly higher tumor growth inhibition with the high dose i.v. AS[S]ODN protocol, as compared to the low-dose treatment. Second, IGF-IR expression was inhibited in tumors from mice receiving AS[S]ODNs as compared to tumors from control groups. Our findings have provided the first evidence that two major signal transduction pathways known to be activated by IGF-IR, the PI-3K/Akt and the classical p42/p44 MAPK pathways (Scrimgeour *et al*., 1997 and references within, Sasaoka *et al*., 1994), were abolished by *in vivo* treatment of mammary tumors with IGF-IR AS[S]ODNs. The PI-3K/Akt pathway originates from the interaction of IGF-IR with one of its major substrates, IRS-1 (Backer *et al*., 1993), whose tyrosine phosphorylation we found significantly lower in C4HD tumors from AS[S]ODN-treated mice as compared to tumors growing in control groups. On the other hand, IGF-IR activates the MAPK/Erk signaling pathway, mainly through the Shc proteins, another IGF-IR key substrate (Sasaoka *et al*., 1994; Scrimgeour *et al*., 1997). Our results are in accordance with recent findings (Peruzzi *et al*., 1999; Navarro and Baserga, 2001) showing that IGF-IR has at least three survival signals that are able to protect 32D murine hemopoietic cells from apoptosis, the PI-3K/Akt, the MAPK/Erk signaling pathways and a third one that results in the mitocondrial translocation of Raf 1, refered to as the 14.3.3 pathway. Simultaneous inactivation of two of these pathways is required to inhibit IGF-IR capacity to protect cells from apoptotic injuries. Therefore, we can hypothezise that blockage of two survival pathways achieved by *in vivo* administration of IGF-IR AS[S]ODNs is directly involved in the successful inhibition of C4HD breast tumor growth. Histological evaluation of tumors from AS[S]ODN-treated mice revealed a great percentage of necrosis. We were not able to define the presence of apoptosis induced by AS[S]ODN treatment using the TdT-mediated dUTP-biotin nick end labeling (TUNEL) method (data not shown). To some extent this was an unexpected result since in many strategies involving downregulation or functional impairment of the IGF-IR, massive apoptosis of tumor cells was found (Resnicoff *et al*., 1995a, b). Several explanations may be attempted. First, the rapidity of the death process makes it difficult to visualize and to quantify apoptosis. Our samples were tumors that developed in mice treated for 14 days with AS[S]ODNs. Withesell and co-workers (Liu *et al*., 1998) have reported results in the N2A mouse neuroblastoma cells that can provide an explanation to our findings. Transfection of N2A cells with IGF-IR antisense plasmids resulted in increase in apoptotic cells detectable at 36 h, followed by marked accumulation of necrotic cells at 48 h (Liu *et al*., 1998). These results are consistent with a mechanism of cell death in which IGF-IR AS[S]ODNs induced apoptotic cell death followed by necrotic degradation of the apoptotic cells. Therefore, this latter phenomenon might apply to what we observe in our tumor samples. Nevertheless, the possibility that the prolonged and sustained abrogation of IGF-IR expression and signaling through PI-3K/Akt and p42/p44 MAPK, and the simultaneous blockage of ErbBs activation might both have led directly to cell death by necrosis.

One of the most exciting findings of our present work is that we were able to demonstrate *in vivo*, what we had already found *in vitro*: the hierarchical interaction between IGF-IR and ErbB-2, by means of which IGF-IR directs ErbB-2 activation (Balana *et al*., 2001). In fact, we extended our results to show that IGF-IR AS[S]ODN-treatment also resulted in significant decrease in the degree of ErbB-3 activation and in the amount of ErbB-2/ErbB-3 heterodimers. Our results are in line with a series of findings that have shown the involvement of IGF-IR in ErbBs signaling pathways (Coppola *et al*., 1994; Ram *et al*., 1996; Swantek and Baserga, 1999). Our findings indicating that *in vivo* IGF-IR blockage in breast cancer cells results in the inactivation of ErbBs has significant therapeutical implications since it indicates that by targeting IGF-IR in breast cancer one might also achieve inhibition of ErbBs activity even in cells overexpressing ErbB-2, such as C4HD. The importance of the functional interaction between IGF-IR and ErbBs in the design of molecular strategies to block tumor growth has also been highlighted by recent findings showing that IGF-IR is able to mediate resistance to anti-EGF-R therapy in human glioblastoma cells through activation of PI-3K/Akt pathway (Chakravarti *et al*., 2002).

We achieved a significant but not complete inhibition of C4HD tumor growth by IGF-IR AS[S]ODN administration, indicating that certain signaling pathways involved in C4HD cell proliferation remained unaffected by blockage of IGF-IR. Since progestins are the main proliferative stimulus in C4HD cells, the first target we explored was the PR. As measure of PR activation, we studied PR Ser294 phosphorylation state,

since a series of recent findings showed that phosphorylation of PR on Ser294 directly correlated with PR transcriptional activity (Lange *et al*., 2000; Shen *et al*., 2001). PR phosphorylation on Ser294 was detected in C4HD tumors from control groups, extending our previous *in vitro* findings which demonstrated that MPA was able to induce PR Ser294 phosphorylation (Labriola *et al*., 2003). Tumors from AS[S]ODN-treated mice of both intratumoral and intravenous protocols showed levels of Ser294 phosphorylation comparable to those found in control groups. Several interesting conclusions on interaction between PR and IGF-IR signaling, and on the role of MAPK on PR Ser294 phosphorylation can be drawn from this result. First, *in vivo* abrogation of IGF-IR expression in the continuous presence of progestins has no effect on PR activity, thereby indicating that the slow proliferation of C4HD tumors after AS[S]ODN administration proceeds through a pathway driven by PR, which is IGF-IR and ErbBs-independent. Second, since abrogation of IGF-IR expression resulted in inhibition of MAPKs activity (Figure 8), our finding provides further support to the most recent findings by Lange and co-workers suggesting that ligand-induced PR Ser294 phosphorylation occurs via MAPK-independent pathways (Qiu *et al*., 2003). In line with these observations, we have recently found that MAPK activity is not required for ligand-induced PR activity (Labriola *et al*., 2003).

In summary, we have for the first time demonstrated that breast cancer growth can be inhibited by either direct intratumor injection or systemic administration of AS[S]ODNs to IGF-IR mRNA. The fact that significant though incomplete inhibition of breast tumor growth was achieved by targeting IGF-IR adds further support to increasing evidence, indicating that more than one targeted therapy is required to achieve full blockage of the multiple signaling pathways used by breast tumors to proliferate. Our finding that PR function remains unaffected by targeting IGF-IR, highlights the importance that a better understanding of the network of pathways involved in breast cancer growth will necessarily have to be developed in the design of therapeutic strategies.

Materials and methods

Animals and tumors

Experiments were carried out in virgin female Balb/c mice raised at the Institute of Biology and Experimental Medicine (IBYME) of Buenos Aires. All animal studies were conducted in accordance with the highest standards of animal care as outlined in the NIH guide for the Care and Use of Laboratory Animals and were approved by the IBYME Animal Research Committee. Hormone-dependent ductal tumor line C4HD originated in mice treated with 40 mg MPA every 3 months for 1 year, and has been maintained by serial transplantation in animals treated with 40 mg s.c. MPA depot in the opposite flank to tumor inoculum (Elizalde *et al*., 1998; Balana *et al*., 1999, 2001). C4HD tumor line is of ductal origin and expresses PR and ER (Elizalde *et al*., 1998; Balana *et al*., 1999, 2001).

ODNs and [S]ODNs

Type I IGF-IR antisense oligodeoxynucleotide (5′ TCC TCC GGA GCC AGA CTT), either phosphodiester (ASODN) or phosphorothioate (AS[S]ODN), comprises a sequence complementary to codons −29 to −24 of the signal sequence of human IGF-IR precursor (Resnicoff *et al*., 1994a). Sense phosphodiester (SODN) or phosphorothioate (S[S]ODN) oligodeoxynucleotides (5′ AAG TCT GGC TCC GGA GGA) were used as controls. ODN and [S]ODN were purchased from Biognostik (Goettingen, Germany).

Cell cultures and proliferation assays

Primary cultures of epithelial cells from C4HD tumors, growing in MPA-treated mice, were performed as previously described (Elizalde *et al*., 1998; Balana *et al*., 1999, 2001). Epithelial cells were plated in culture flasks with DMEM/F12 + 5% steroid-stripped fetal calf serum (ChFCS, Gen S.A., Buenos Aires), and allowed to attach for 24–48 h. Purity of epithelial cultures was evaluated by cytokeratin staining. Cells were incubated in DMEM/F12 (without phenol red, with 100 U/ml penicillin and with 100 μ/ml streptomycin), with 2.5% ChFCS in the presence of MPA 10 nM and the indicated concentrations of either phosphodiester or phosphorothioate ODNs. After a 24 h incubation, 50% of media was replaced by fresh media, and cells were incubated for another 24 h in the presence of 0.8 μCi (^{3}H)-thymidine (NEN, Dupont, Boston, MA, USA; specific activity: 70–90Ci/mmol). Cells were then trypsinized and harvested. Assays were performed in octuplicate. The differences between control and experimental groups were analysed by ANOVA followed by Tukey *t*-test between groups. In former experiments we had demonstrated that thymidine uptake correlates with the number of cells/well (Elizalde *et al*., 1998; Balana *et al*., 1999, 2001).

Intratumor and systemic administration of [S]ODNs

Mice were inoculated s.c. into the left flank with a fragment of C4HD tumor (1 mm^3) and with the MPA pellet into the other flank. Tumor growth was measured daily with a Vernier caliper. Tumor volume (mm^3) was calculated as $(L \times W^2)/2$, where L is the length (mm) and W the width (mm). [S]ODNs treatment was initiated when the tumor reached a mean of volume of 15 mm^3 (approximately 1 week after inoculum). In the intratumor protocol, mice were injected directly into the tumor with 100 μg/day/mouse IGF-IR AS[S]ODNs, S[S]ODNs (dissolved in 100 μl of PBS) or PBS for 14 days. To test the effect of systemic administration of AS[S]ODNs, in the first protocol (low-dose), mice were injected i.v. via the retroorbital venous sinus with 0.25 mg/day/mouse AS[S]ODN, [S]ODN or 100 μl PBS for 7 days. Then, dose was raised to 1 mg/day/mouse of AS[S]ODN or S[S]ODN on days 8, 10, 12 and 14 and to 0.5 mg/day/mouse of oligonucleotides on days 9, 11 and 13. In the second systemic protocol (high-dose), mice were injected with 1 mg/day/mouse AS[S]ODN, [S]ODN or 100 μl PBS from day 1 to day 14 of treatment. Tumor width and length were measured daily, in order to calculate volume. Tumor growth rates were determined as the slopes of growth curves. The percentage of tumor growth inhibition was calculated by dividing the mean tumor volume of the AS[S]ODN-treated group by the mean tumor volume of control groups, subtracting the resulting value from 1, and multiplying it by 100. Tumor growth delay was evaluated as T−C, where T and C are the median times for treated and control tumors respectively, to reach the same volume. At day 15, half the animals from each group in all three experimental protocols were killed and tumors were removed. Tissues to be used for molecular studies were stored at −80°C

and tissues for histophatological analysis were fixed in 10% buffered formalin. The other half of mice in each experimental group was kept alive for one more week after the end of the treatment. Samples of liver, lung, heart and pancreas were also fixed for histological examination. Comparison of tumor volumes between the different groups during specific times was made by ANOVA followed by Tukey *t*-test between groups. Linear regression analysis was performed on tumor growth curves, and the slopes were compared using ANOVA followed by parallelism test to evaluate the statistical significance of the differences.

Histophatological analysis

Tumors were excised and fixed in 10% buffered formalin. Representative fragments were embedded in parafin, 5 μm sections were obtained and stained with H&E for microscopic observations.

Serum levels of glucose, creatinine, ALT and AST

The levels of glucose, creatinine, alanine aminotrasferase (ALT) and AST were measured using and Auto-Biochemical Analyzer (Autolab, Roche, Basel Switzerland) in serum samples collected at day 15 in each experimental protocol. Blood samples were taken by retroorbital bleeding.

IGF-IR, IRS-1, AKT, ErbB-2, ErbB-3, MAPK, and PR expression and activation

Protein lysates from C4HD tumors growing in mice subjected to different treatments were prepared as previously described (Elizalde *et al*., 1998; Balana *et al*., 1999, 2001). Proteins were solubilized in sample buffer (60 mM Tris-HCl, pH 6.8, 2% SDS, 10% glycerol and 0.01% bromophenol blue) and subjected to SDS–PAGE. Proteins were electroblotted onto nitrocellulose. Membranes were immunoblotted with the following antibodies: IGF-IRα (sc-712), ErbB-2 (Neu C-18), ErbB-3 (C-17), anti-total p42/p44 MAPK (C-14), anti-phospho p42/p44 MAPK (E-4) and actin (C-2), all from Santa Cruz Biotechnology (Santa Cruz, CA, USA), IGF-Iβ (Ab-5), phospho-294-PR Ab-12 (clone 608) and hPR Ab-7 (clone 7) from Neomarkers (Freemont, CA, USA), total Akt, phospho Akt (Thr308) and phospho Akt (Ser 473) from Cell Signaling (Beverly, MA, USA). After washing, membranes were incubated with HRP-conjugated secondary antibody (Amersham International, UK). Enhanced chemiluminescence (ECL) was performed according to the manufacturer's instructions (Amersham). To perform IRS-1, ErbB-2 and ErbB-3 tyrosine phosphorylation analysis, cell lysates (500 μg protein) were precleared with Protein A-Agarose (Santa Cruz Biotechnology). In total, 2–5 μg of each primary antibody was used in each immunoprecipitation, which was rocked for 2 h at 4°C. Thereafter, the immunocomplexes were captured by adding Protein A-Agarose and rocked for an additional 2 h. Beads were washed three times with lysis buffer, then boiled for 10 min in sample buffer and subjected to SDS–PAGE on a 6% gel. Proteins were electroblotted onto nitrocellulose and filters were probed with mouse monoclonal Anti-P-Tyr PY-99 (Santa Cruz Biotechnology). Differences in protein expression and activation between control and experimental groups were analysed by paired *t*-test.

Acknowledgements
This work was supported by grants from Lilly Centre for Women's Health, Eli Lilly and Company and from the Centro Argentino Brasilero de Biotecnología (CABBIO), both awarded to PV Elizalde, and by grant IDB 802/OC-AR PICT 0503402 from the National Agency of Scientific Promotion of Argentina. We thank N Lope for her expert assistance with animal care and C Lanari for providing the MPA-induced mammary tumor model.

References

Adeyinka A, Nui Y, Cherlet T, Snell L, Watson PH and Murphy LC. (2002). *Clin. Cancer Res.*, **8,** 1747–1753.
Arteaga CL and Osborne CK. (1989). *Cancer Res.*, **49,** 6237–6241.
Backer JM, Myers Jr MG, Sun XJ, Chin DJ, Shoelson SE, Miralpeix M and White MF. (1993). *J. Biol. Chem.*, **268,** 8204–8212.
Balana ME, Labriola L, Salatino M, Movsichoff F, Peters G, Charreau EH and Elizalde PV. (2001). *Oncogene*, **20,** 34–47.
Balana ME, Lupu R, Labriola L, Charreau EH and Elizalde PV. (1999). *Oncogene*, **18,** 6370–6379.
Baserga R. (1999). *Exp. Cell Res.*, **253,** 1–6.
Boonyaratanakornkit V, Scott MP, Ribon V, Sherman L, Anderson SM, Maller JL, Miller WT and Edwards DP. (2001). *Mol. Cell*, **8,** 269–280.
Burfeind P, Chernicky CL, Rininsland F, Ilan J and Ilan J. (1996). *Proc. Natl. Acad. Sci. USA*, **93,** 7263–7268.
Chakravarti A, Loeffler JS and Dyson NJ. (2002). *Cancer Res.*, **62,** 200–207.
Chernicky CL, Tan H, Yi L, Loret de Mola JR and Ilan J. (2002). *Mol. Pathol.*, **55,** 102–109.
Chernicky CL, Yi L, Tan H, Gan SU and Ilan J. (2000). *Cancer Gene Ther.*, **7,** 384–395.
Cho H, Aronica SM and Katzenellenbogen BS. (1994). *Endocrinology*, **134,** 658–664.
Clemm DL, Sherman L, Boonyaratanakornkit V, Schrader WT, Weigel NL and Edwards DP. (2000). *Mol. Endocrinol.*, **14,** 52–65.
Coppola D, Ferber A, Miura M, Sell C, D'Ambrosio C, Rubin R and Baserga R. (1994). *Mol. Cell. Biol.*, **14,** 4588–4595.
Cui X, Zhang P, Deng W, Oesterreich S, Lu Y, Mills GB and Lee AV. (2003). *Mol. Endocrinol.*, **17,** 575–588.
Dunn SE, Ehrlich M, Sharp NJ, Reiss K, Solomon G, Hawkins R, Baserga R and Barrett JC. (1998). *Cancer Res.*, **58,** 3353–3361.
Elizalde PV, Lanari C, Molinolo AA, Guerra FK, Balana ME, Simian M, Iribarren AM and Charreau EH. (1998). *J. Steroid Biochem. Mol. Biol.*, **67,** 305–317.
Ignar-Trowbridge DM, Nelson KG, Bidwell MC, Curtis SW, Washburn TF, McLachlan JA and Korach KS. (1992). *Proc. Natl. Acad. Sci. USA*, **89,** 4658–4662.
Katzenellenbogen BS and Norman MJ. (1990). *Endocrinology*, **126,** 891–898.
Labriola L, Salatino M, Proietti CJ, Pecci A, Coso OA, Kornblihtt AR, Charreau EH and Elizalde PV. (2003). *Mol. Cell. Biol.*, **23,** 1095–1111.
Lange CA, Richer JK, Shen T and Horwitz KB. (1998). *J. Biol. Chem.*, **273,** 31308–31316.
Lange CA, Shen T and Horwitz KB. (2000). *Proc. Natl. Acad. Sci. USA*, **97,** 1032–1037.

Lee AV, Jackson JG, Gooch JL, Hilsenbeck SG, Coronado-Heinsohn E, Osborne CK and Yee D. (1999). *Mol. Endocrinol.*, **13,** 787–796.

Lee CT, Park KH, Adachi Y, Seol JY, Yoo CG, Kim YW, Han SK, Shim YS, Coffee K, Dikov MM and Carbone DP. (2003). *Cancer Gene Ther.*, **10,** 57–63.

Lee CT, Wu S, Gabrilovich D, Chen H, Nadaf-Rahrov S, Ciernik IF and Carbone DP. (1996). *Cancer Res.*, **56,** 3038–3041.

Li W, Hyun T, Heller M, Yam A, Flechner L, Pierce JH and Rudikoff S. (2000). *Cancer Res.*, **60,** 3909–3915.

Liu X, Turbyville T, Fritz A and Whitesell L. (1998). *Cancer Res.*, **58,** 5432–5438.

Migliaccio A, Piccolo D, Castoria G, Di Domenico M, Bilancio A, Lombardi M, Gong W, Beato M and Auricchio F. (1998). *EMBO J.*, **17,** 2008–2018.

Nabel GJ, Nabel EG, Yang ZY, Fox BA, Plautz GE, Gao X, Huang L, Shu S, Gordon D and Chang AE. (1993). *Proc. Natl. Acad. Sci. USA*, **90,** 11307–11311.

Nakamura K, Hongo A, Kodama J, Miyagi Y, Yoshinouchi M and Kudo T. (2000). *Cancer Res.*, **60,** 760–765.

Navarro M and Baserga R. (2001). *Endocrinology*, **142,** 1073–1081.

Neuenschwander S, Roberts Jr CT and LeRoith D. (1995). *Endocrinology*, **136,** 4298–4303.

Oesterreich S, Zhang P, Guler RL, Sun X, Curran EM, Welshons WV, Osborne CK and Lee AV. (2001). *Cancer Res.*, **61,** 5771–5777.

Peruzzi F, Prisco M, Dews M, Salomoni P, Grassilli E, Romano G, Calabretta B and Baserga R. (1999). *Mol. Cell. Biol.*, **19,** 7203–7215.

Pietras RJ, Arboleda J, Reese DM, Wongvipat N, Pegram MD, Ramos L, Gorman CM, Parker MG, Sliwkowski MX and Slamon DJ. (1995). *Oncogene*, **10,** 2435–2446.

Plautz GE, Yang ZY, Wu BY, Gao X, Huang L and Nabel GJ. (1993). *Proc. Natl. Acad. Sci. USA*, **90,** 4645–4649.

Prager D, Li HL, Asa S and Melmed S. (1994). *Proc. Natl. Acad. Sci. USA*, **91,** 2181–2185.

Qiu M, Olsen A, Faivre E, Horwitz KB and Lange CA. (2003). *Mol. Endocrinol.*, **17,** 628–642.

Ram TG, Dilts CA, Dziubinski ML, Pierce LJ and Ethier SP. (1996). *Mol. Carcinog.*, **15,** 227–238.

Resnicoff M, Abraham D, Yutanawiboonchai W, Rotman HL, Kajstura J, Rubin R, Zoltick P and Baserga R. (1995a). *Cancer Res.*, **55,** 2463–2469.

Resnicoff M, Burgaud JL, Rotman HL, Abraham D and Baserga R. (1995b). *Cancer Res.*, **55,** 3739–3741.

Resnicoff M, Coppola D, Sell C, Rubin R, Ferrone S and Baserga R. (1994a). *Cancer Res.*, **54,** 4848–4850.

Resnicoff M, Sell C, Rubini M, Coppola D, Ambrose D, Baserga R and Rubin R. (1994b). *Cancer Res.*, **54,** 2218–2222.

Rohlik QT, Adams D, Kull Jr FC and Jacobs S. (1987). *Biochem. Biophys. Res. Commun.*, **149,** 276–281.

Sasaoka T, Rose DW, Jhun BH, Saltiel AR, Draznin B and Olefsky JM. (1994). *J. Biol. Chem.*, **269,** 13689–13694.

Scrimgeour AG, Blakesley VA, Stannard BS and LeRoith D. (1997). *Endocrinology*, **138,** 2552–2558.

Sell C, Dumenil G, Deveaud C, Miura M, Coppola D, DeAngelis T, Rubin R, Efstratiadis A and Baserga R. (1994). *Mol. Cell. Biol.*, **14,** 3604–3612.

Shen T, Horwitz KB and Lange CA. (2001). *Mol. Cell. Biol.*, **21,** 6122–6131.

Stewart AJ, Johnson MD, May FE and Westley BR. (1990). *J. Biol. Chem.*, **265,** 21172–21178.

Surmacz E, Guvakova MA, Nolan MK, Nicosia RF and Sciacca L. (1998). *Breast Cancer Res. Treat.*, **47,** 255–267.

Swantek JL and Baserga R. (1999). *Endocrinology*, **140,** 3163–3169.

Tamm I, Dorken B and Hartmann G. (2001). *Lancet*, **358,** 489–497.

Werner H and Le Roith D. (2000). *Cell Mol. Life Sci.*, **57,** 932–942.

Yu H and Rohan T. (2000). *J. Natl. Cancer Inst.*, **92,** 1472–1489.